Polyamidoxime Chain Length Drives Emergent Metal-Binding Phenomena

Lyndsey D. Earl,[†∥] Changwoo Do,[§]* Yangyang Wang,[‡] Carter W. Abney[†]*

† Chemical Sciences Division, Physical Sciences Directorate, Oak Ridge National Laboratory, One Bethel Valley Road, P.O. Box 2008, Oak Ridge, TN 37831, U.S.A

§ Neutron Scattering Division, Oak Ridge National Laboratory, One Bethel Valley Road, P.O. Box 2008, Oak Ridge, TN 37831, U.S.A.

‡ Center for Nanophase Materials Sciences, Physical Sciences Directorate, Oak Ridge National Laboratory, One Bethel Valley Road, P.O. Box 2008, Oak Ridge, TN 37831, U.S.A

AUTHOR INFORMATION

Corresponding Author

* Changwoo Do, doc1@ornl.gov

* Carter W. Abney, abneycw@ornl.gov

Table of contents

Materials synthesis

Acetamidoxime was prepared according to a previously reported procedure.[1] All chemicals were obtained from Sigma-Aldrich. Acrylonitrile was passed through a column of inhibitor remover prior to use. 2,2′-Azobis(2-methylpropionitrile) was recrystallized from methanol.

Polyacrylonitrile (PAN): The protocol for the synthesis of low molecular weight polyamidoxime using radical addition-fragmentation chain-transfer (RAFT) polymerization was adapted from previously reported procedures.[2-3] A solution of 4-cyano-4-(phenylcarbonothioylthio)pentanoic acid (0.050 g, 0.18 mmol) and 2,2′-azobis(2-methylpropionitrile) (0.010 g, 0.061 mmol) in acrylonitrile (2.0 mL, 30 mmol) and anhydrous DMF (4.0 mL) was transferred to a dry 25 mL Schlenk tube charged with a magnetic stir bar. The reaction vessel was subjected to three freeze-pump-thaw cycles and backfilled with argon at room temperature. The reaction vessel was sealed, subjected to magnetic stirring, and heated at 68-71 ºC (oil bath temperature) during the reaction (see Table S1). After 20-30 minutes, the solution changed from red-pink to orange. The reaction was quenched by placing the reaction vessel in a water-ice bath and exposing the mixture to air. Addition of 2:1 water:methanol (35 mL) precipitated PAN, and the suspension was centrifuged. Two additional wash and centrifugation cycles resulted in a light pink solid. The solid was dried for 24 hours under house vacuum at 40 ºC followed by drying at < 100 mT at room temperature for at least 24 hours.

Table S1 Reaction times and recovered mass of PAN.

Polymer	Reaction time (hr)	Isolated mass (g)
PAN (n = 10)	1	0.0800
PAN (n = 30)	2	0.1636
PAN (n = 125)	18	1.2870

Polyamidoxime (PAO): PAN (see Table S2) was pulverized using a mortar and pestle and dissolved in a freshly prepared solution of 5% NH_2OH in 1:1 $DMSO:H_2O$ (15 mL). In addition to converting the nitrile to amidoxime, the dithiocarboxylic acid ester is converted to a thiol upon treatment with hydroxylamine. The solution was stirred at room temperature for 48-96 hours during which time the solution color changed from red-orange to light yellow or colorless. Water (30 mL) was slowly added with stirring, and a white precipitate formed. The solid was isolated by centrifugation and washed two additional times with water by centrifugation and once with methanol. The white solid was dried for 24 hours under house vacuum at 40 ºC followed by drying at < 100 mT at room temperature for 40 hours.

Table S2 Mass of PAN used in amidoximation reaction and isolated mass of PAO

Polymer	PAN mass (g)	Isolated mass (g)
n = 10	0.0500	0.0413
n = 30	0.1008	0.0867
n = 125	0.1959	0.1973

Materials characterization

Infrared spectra were collected from 650-4000 cm^{-1} (4 cm^{-1} resolution, 8 scans) on PerkinElmer Frontier FT-IR spectrometer with a Universal ATR Sampling Accessory. ^{1}H NMR were collected on a Bruker Avance 400 at 400 MHz and referenced to reference solvent ((CD_3)$_2$SO, 2.50 ppm). Size exclusion chromatography elutograms were collected using a Waters 2695 Alliance HPLC pump equipped with degasser and autosampler, 3 X Polymer Labs Mixed-C Ultrapolystryagel columns in a thermostatted compartment, a Wyatt miniDAWN 3-angle ambient light scattering detector, and a Waters 2414 refractive index detector. 0.05M LiBr in DMF was used as the eluent at a 0.5 mL min^{-1} flow rate with the columns at 60 °C. Molecular weight values were obtained using Wyatt Astra software. 3rd-order polynomial calibrations were made by using poly-2-vinylpyridine standards passed in the same run as the analytes to verify calibration durability.
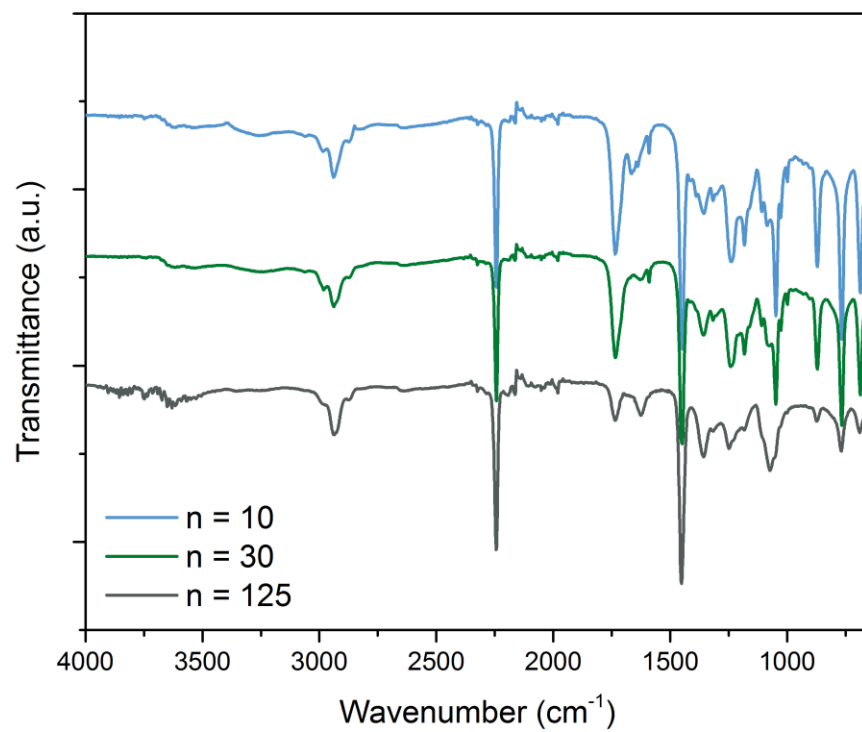
Figure S1 Infrared spectra of PAN precursors.
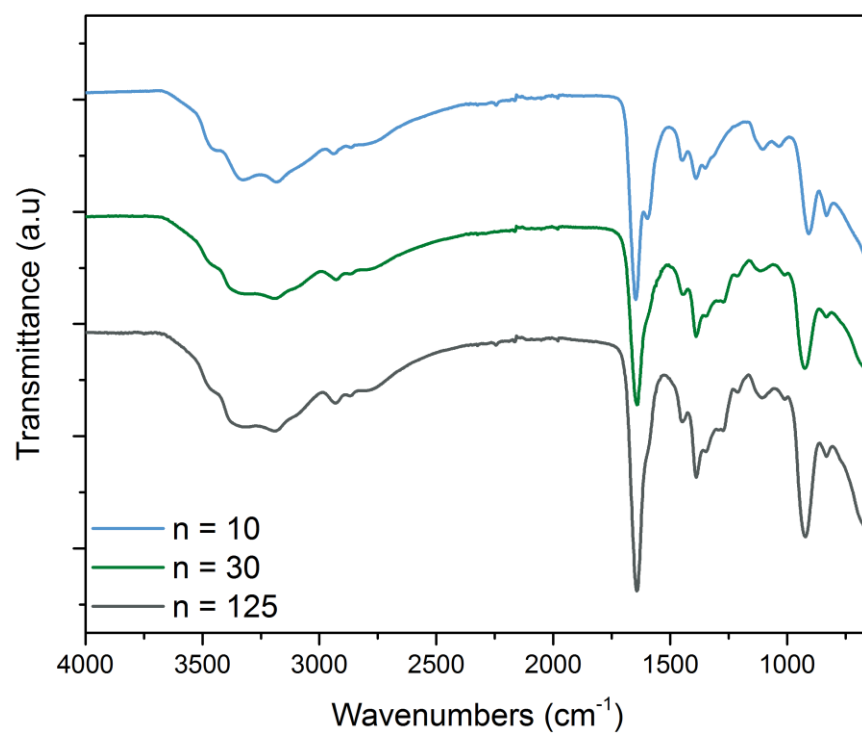
Figure S2 Infrared spectra of polyamidoximes.
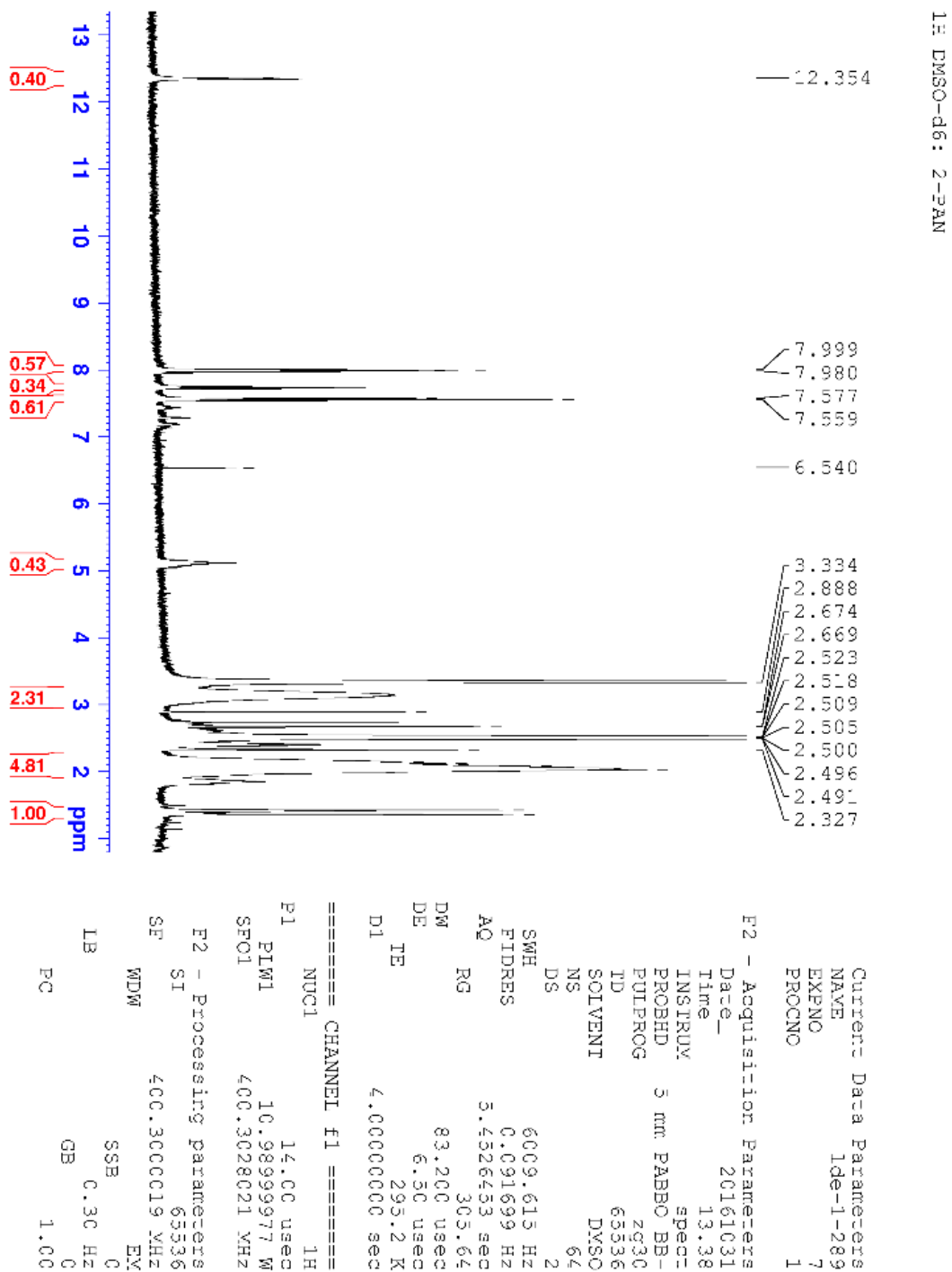
Figure S3 ^{1}H NMR of short PAN oligomer (n = 10) in DMSO-d$_6$
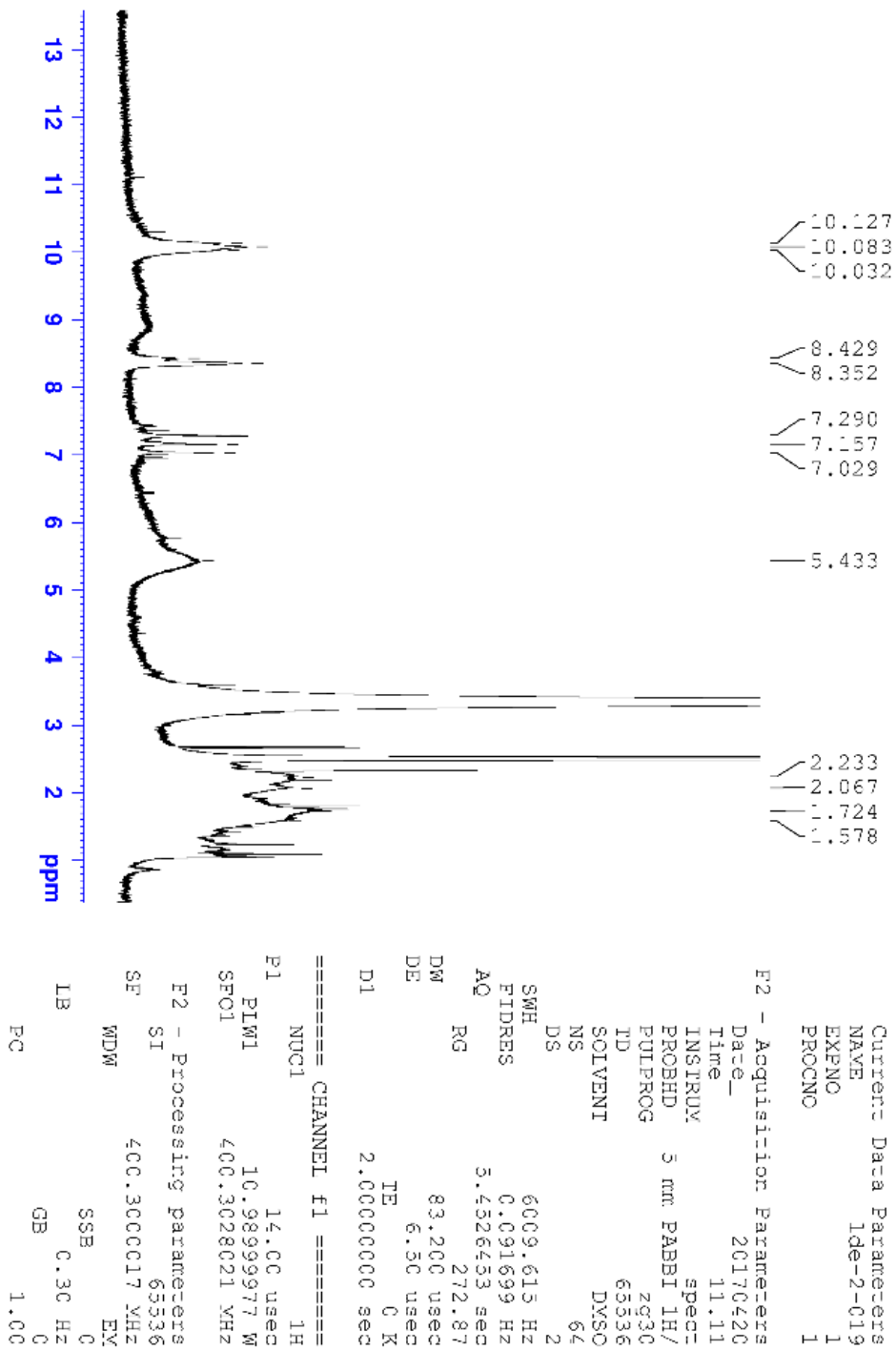
Figure S4 ^{1}H NMR of short polyamidoxime oligomer (n = 10) in DMSO-d6
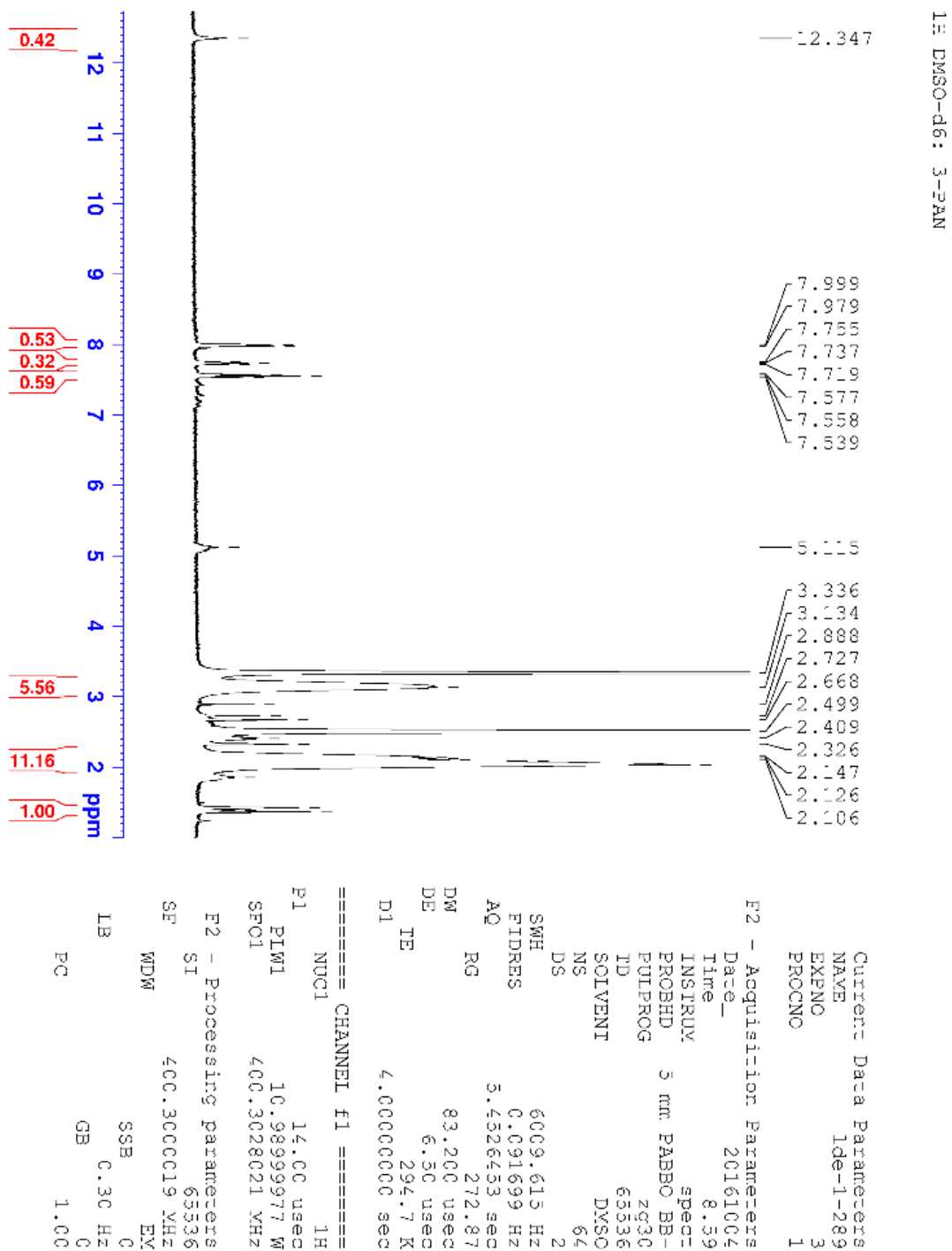
Figure S5 ^{1}H NMR of intermediate PAN (n = 30) in DMSO-d$_6$
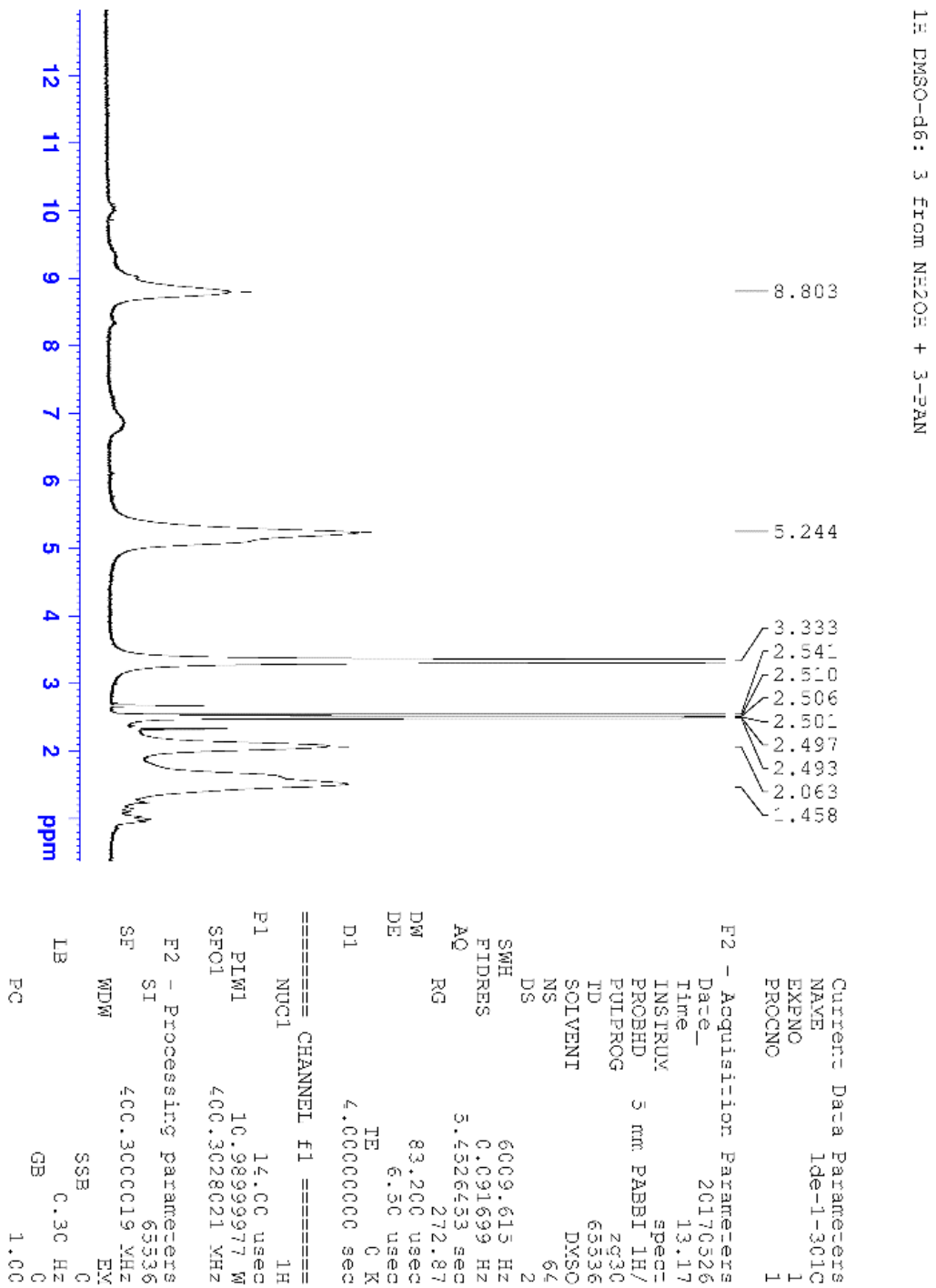
Figure S6 ^{1}H NMR of intermediate polyamidoxime oligomer (n = 30) in DMSO-d₆

Figure S7 ^{1}H NMR of long PAN (n = 125) in DMSO-d$_6$.
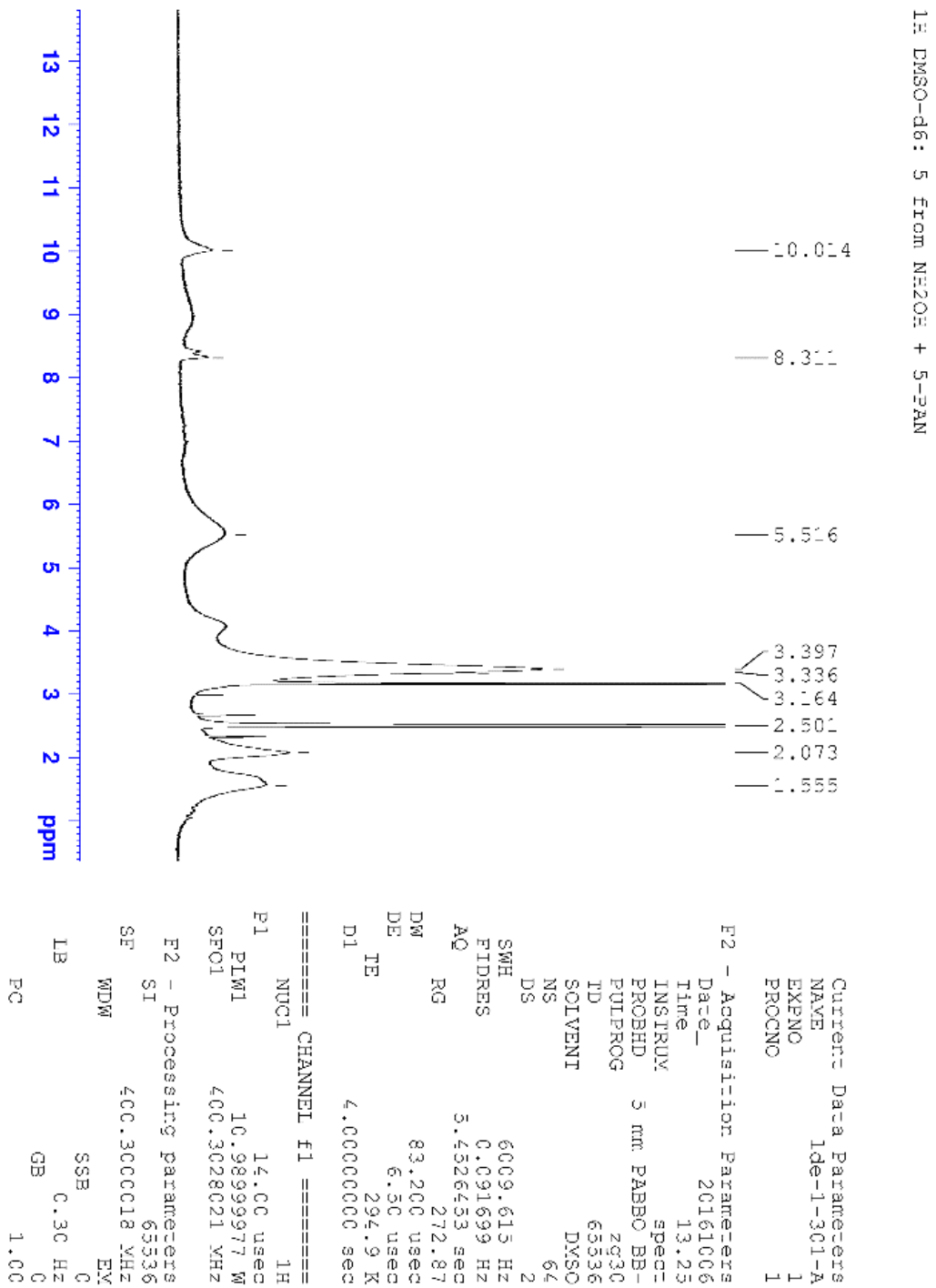
Figure S8 ^{1}H NMR of long polyamidoxime oligomer (n = 125) in DMSO-d₆.
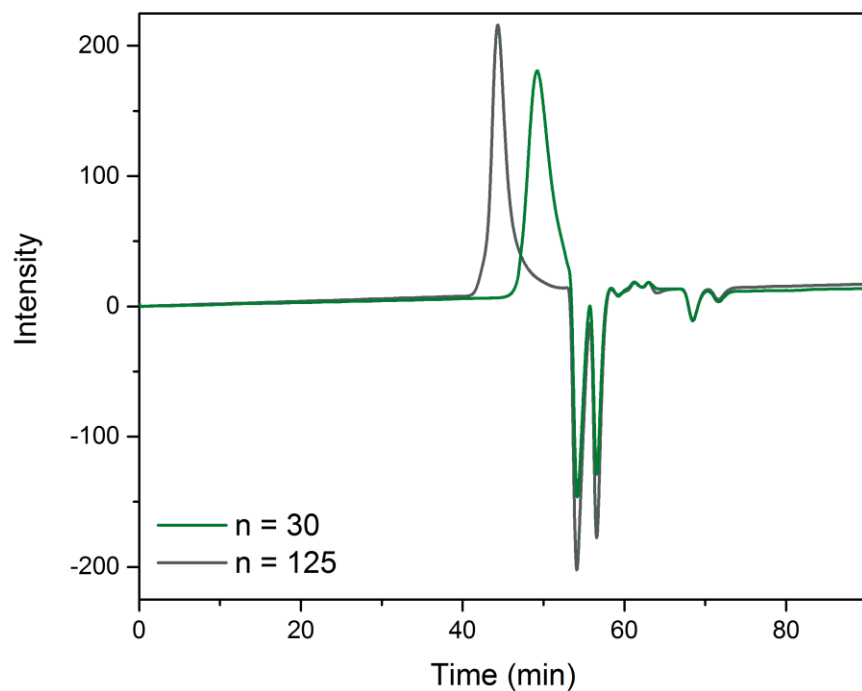
Figure S9 Size exclusion chromatography elutograms of polyacrylonitrile precursors in 0.05 M LiBr in DMF
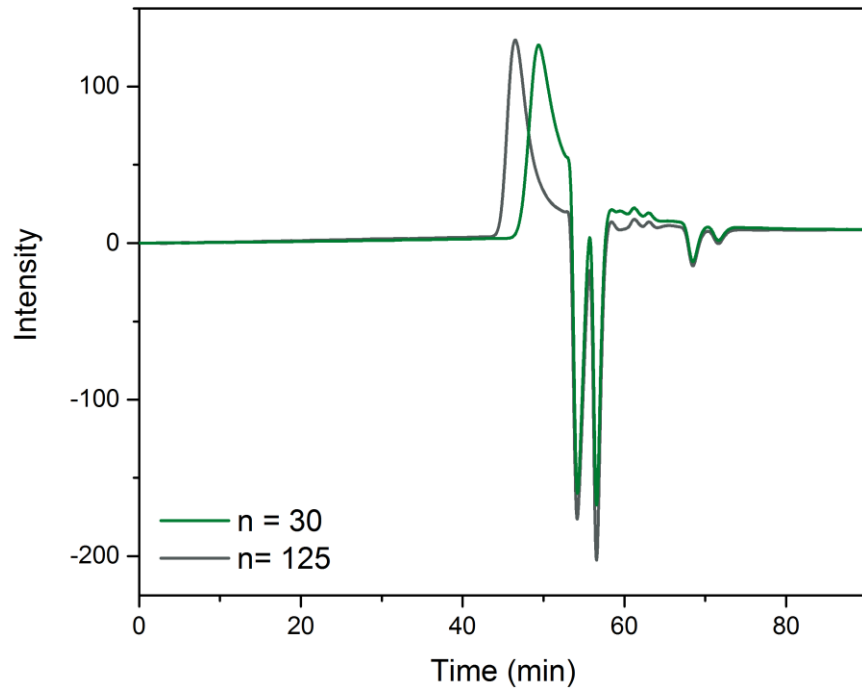
Figure S10 Size exclusion chromatography elutograms of polyamidoximes in 0.05 M LiBr in DMF.

Table S3 Molecular weight summary of polyacrylonitriles and polyamidoximes obtained from size exclusion chromatography elutograms.

Sample	M_n	M_w	PDI
Intermediate PAN (n = 30)	3721	4371	1.17
Long-PAN (n = 125)	13796	16693	1.21
Intermediate polyamiodxime (n = 30)	3238	3909	1.20
Long polyamidoxime (n = 125)	6664	8470	1.27

X-ray Absorption Fine Structure (XAFS) Spectroscopy

Solutions prepared for XAFS spectroscopy experiments contained 5 mM $UO_2(NO_3)_2 \cdot 6\ H_2O$ and 25 mM amidoxime binding sites in DMSO (~3 mg/mL polymer). Solutions were placed in disposable polystyrene cuvettes.

XAFS spectra were collected at Stanford Synchrotron Radiation Lightsource (SSRL), Beamline 11-2. Spectra were collected at the uranium L_{III}-edge (17166 eV). Data were collected by a 100-pixel monolithic solid state Ge fluorescence detector. The X-ray was monochromatized by a Si(220) monochromator and detuned using Rh-coated mirrors to eliminate higher order harmonics. The K-edge of an Y-foil (17038 eV) was used as the reference for energy calibration and measured simultaneously. Three scans were collected for each sample. All data were collected at room temperature.

Samples were centered on the beam prior to data collection (beam size 1 mm × 0.5 mm). The incident beam intensity (I_0) and transmitted beam intensity (I_t) were measured by ionization

chambers with 100% N_2 gas composition. Data were collected in four regions, with all energies listed relative to the environmental U L_{III}-edge (17166 eV): -230 to -30 eV (10 eV step size, 0.25 s dwell time), -30 to -5 eV (5 eV step size, 0.5 s dwell time), -5 to 30 eV (1 eV step size), 3 $Å^{-1}$ to 15 $Å^{-1}$ (0.05 Å-1 step size), with dwell time increasing as a function of k from 2.0 s at 3 $Å^{-1}$ to 16.0 s at 15 $Å^{-1}$.

The data were reformatted using SixPack[4] then processed and analyzed using the Athena and Artemis programs of the IFEFFIT package based on FEFF 6.[5-6] Reference data were aligned to the first zero-crossing of the second derivative of the normalized μ(E) data, which was subsequently calibrated to the literature E_0 for the U L_{III}-edge (17166 eV). Spectra were averaged in μ(E) prior to normalization. The background was removed and the data were assigned an R_{bkg} value of 0.8.

All data were fit simultaneously with k-weighting of 1,2, and 3, and the final refinement was conducted with a k-weighting of 2. Structural parameters that were determined by the fits include the coordination number of the equatorial oxygen scattering path for each system, the change in half-path length, R_{eff} (ΔR_i), the relative mean square displacement of the scattering element (σ^2_i), the passive electron reduction factor (S_0^2), and the energy shift of the photoelectron, (ΔE_0). Given the minimal variations anticipated for the chemical environment of the axial oxygens of the uranyl cation, the σ^2 parameter for the U $\rightarrow$ O_{ax} scattering path was obtained by fitting the control sample of $UO_2(NO_3)_2$ and fixed for experimental samples. Because the solutions were prepared similarly with respect to the mass concentration of UO_2^{2+} and polymer in solution, S_0^2 was also obtained from the refined fit of the $UO_2(NO_3)_2$ standard. The fit range (ΔR), data range (Δk), number of independent points (N_{idp}), number of variables (N_{var}), reduced chi-squared value (χ_v^2), and R-factor (R) are in Table S4. To adhere to the Nyquist criterion,[7-8] the number of variables did not exceed 2/3 the number of independent points. Coordination numbers were restrained to be $\geq$ 0, and the total number of atoms in the equatorial plane was restrained to be between 4 and 6.5.

Table S4 Metrics for EXAFS fits.

Metric	$UO_2(NO_3)$	n = 1	n = 1	n = 10	n = 30	n = 125
S_0^2	1.00 ± 0.04	1	1	1	1	1
χ_v^2	19.1	57.4	89.5	31.3	34.9	72.6
R-factor	0.6 %	1.1%	1.5 %	1.2 %	0.3 %	1.5 %
R-range	1-3.5	1-3.7	1 – 2.5			
k-range	3.0-12.6	3-12.1	3 – 12.6			
N_{idp}	15.1	15.4	9.0			
N_{var}	10	7	6			

Table S5 Paths, initial path lengths, initial degeneracies and parameters for the fit of the $UO_2(NO_3)_2$ control, obtained from single crystal structures.

Scattering Path	N_{degen}	R (Å)	Δ R (Å)	σ^2 (Å^2)
$U \rightarrow O_{ax}$	2	1.78	---	σ^2-O_{ax}
$U \rightarrow O_{eq}$	6	2.40	ΔR-O	σ^2-O
$U \rightarrow N_1$	1	2.72	ΔR-N	σ^2-N
$U \rightarrow N_2$	1	2.99	ΔR-N	σ^2-N
$U \rightarrow O_{ax(1)} \rightarrow O_{ax(2)}$	2	3.47	---	$2 \times \sigma^2$-O_{ax}
$U \rightarrow O_{ax(1)} \rightarrow U \rightarrow O_{ax(1)}$	2	3.49	---	$2 \times \sigma^2$-O_{ax}
$U \rightarrow O_{ax(1)} \rightarrow U \rightarrow O_{ax(2)}$	2	3.49	---	$2 \times \sigma^2$-O_{ax}
$U \rightarrow S$	1	3.52	ΔR-S	σ^2-S

Table S6 Best fit values for the $UO_2(NO_3)_2$ control.

Scattering Path	N_{degen}	R (Å)	σ^2 ($\times 10^{-3}$ Å^2)
$U \rightarrow O_{ax}$	2[a]	1.78[b]	1.8 ± 0.4
$U \rightarrow O_{eq}$	6[a]	2.37 ± 0.02	9.2 ± 0.9

Scattering Path		R (Å)	σ² (× 10⁻³ Å²)
$U \rightarrow N_1$	1^a	2.88 ± 0.01	2 ± 2
$U \rightarrow N_2$	1^a	3.15 ± 0.01	2 ± 2
$U \rightarrow O_{ax(1)} \rightarrow O_{ax(2)}$	2^a	3.47^b	3.6 ± 0.8
$U \rightarrow O_{ax(1)} \rightarrow U \rightarrow O_{ax(1)}$	2^a	3.49^b	3.6 ± 0.8
$U \rightarrow O_{ax(1)} \rightarrow U \rightarrow O_{ax(2)}$	2^a	3.49^b	3.6 ± 0.8
$U \rightarrow S$	2.3 ± 1.4	3.60 ± 0.02	6 ± 5
$S_0^2 = 1.000 \pm 0.004$			
$\Delta E_0 = 6.8 \pm 0.7$			

[a.] The coordination number was fixed in the fit.
[b.] The bond length was fixed in the fit.

Table S7 Refined values for the fit of the UO$_2$ small molecule system over longer *R*-space, including second shell scattering paths.

Scattering Path	N_{degen}	R (Å)	σ² (× 10⁻³ Å²)
$U \rightarrow O_{ax}$	2^a	1.78^b	2^c
$U \rightarrow O_{eq(short)}$	3.1 ± 0.7	2.31^b	6 ± 2
$U \rightarrow O_{eq(long)}$	2.4 ± 0.6	2.42^b	6 ± 2
$U \rightarrow N_{monodentate}$	1.2 ± 0.7	2.99^b	6 ± 2
$U \rightarrow C_{\eta2}$	2.4 ± 0.6	3.48^b	6 ± 2
$U \rightarrow S$	1.9 ± 0.7	3.53 ± 0.02	7 ± 4
$U \rightarrow O_{ax(1)} \rightarrow O_{ax(2)}$	2	3.55	---
$U \rightarrow O_{ax(1)} \rightarrow U \rightarrow O_{ax(1)}$	2	3.55	---
$U \rightarrow O_{ax(1)} \rightarrow U \rightarrow O_{ax(2)}$	2	3.55	---
$S_0^2 = 1.000$ (Fixed)			
$\Delta E_0 = 8.2 \pm 0.9$			

[a.] The coordination number was fixed in the fit.
[b.] The bond length was fixed in the fit.
[c.] The mean displacement was fixed in the fit.

Table S8 Paths, initial path lengths, initial degeneracies and parameters for the first shell fit of the small molecule system and all polymer samples.

Scattering Path	N_{degen}	R (Å)	Δ R (Å)	σ^2 ($\times$ 10^{-3} Å^2)
U → O$_{ax}$	2	1.78	---	---
U → O$_{eq(short)}$	1	2.31	ΔR-O$_{short}$	σ^2-O
U → O$_{eq(long)}$	4	2.42	ΔR-O$_{long}$	σ^2-O
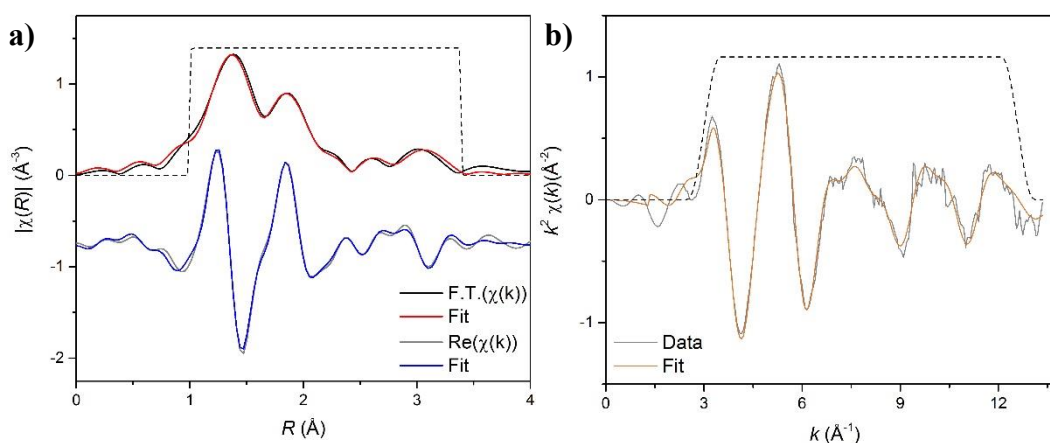
Figure S11 a) Fourier transform of the U L$_{III}$-edge EXAFS spectrum of the UO$_2$(NO$_3$)$_2$ control in R-space and fit (red trace). The real component and fit (blue trace) are presented beneath. b) EXAFS spectrum and fit (orange trace) of the UO$_2$(NO$_3$)$_2$ control in k-space. For both figures, the black dashed line denotes the fit window.
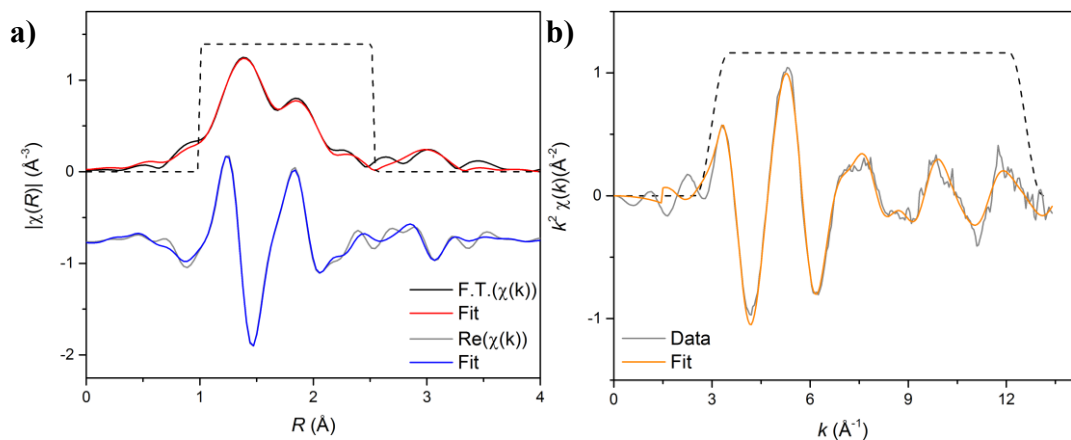
Figure S12 First shell fit for the acetamidoxime small molecule sample (n = 1). The fit window is identical to fits of the polymer systems; longer scattering paths are not included in this fit. a) Fourier transform of the U L_{III}-edge EXAFS spectrum in *R*-space and fit (red trace). The real component and fit (blue trace) are presented beneath. b) EXAFS spectrum and fit (orange trace) of n = 1 in *k*-space with accompanying fit afforded by a two-shell model. For both figures, the black dashed line denotes the fit window.
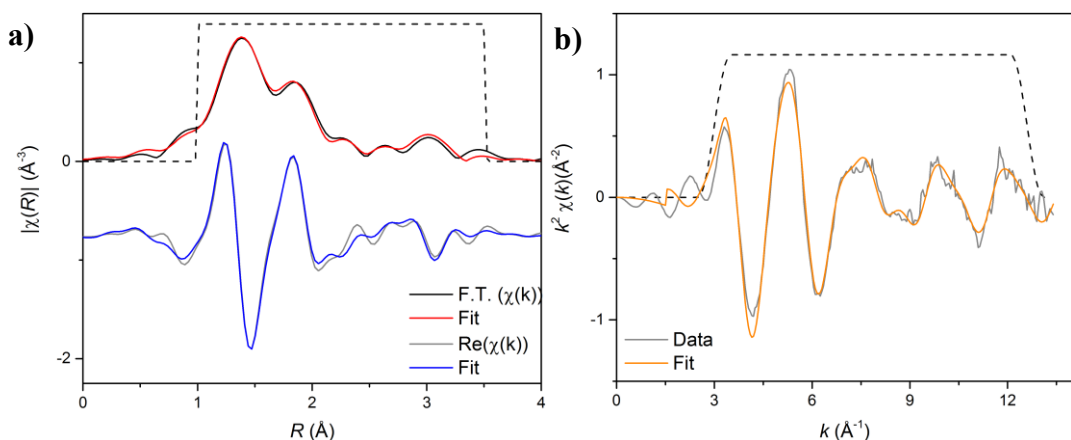
Figure S13 Extended fit for the acetamidoxime small molecule sample (n = 1), including longer scattering paths and multiple scattering paths. a) Fourier transform of the U L_{III}-edge EXAFS spectrum of n = 1, the acetamidoxime small molecule, in *R*-space and fit including U-S_{DMSO} and U-O_{NO3} paths (red trace). The real component and fit (blue trace) are presented beneath. b) Accompanying EXAFS spectrum and fit (orange trace) of n = 1 in k-space with accompanying fit afforded by a two-shell model. For both figures, the black dashed line denotes the fit window.
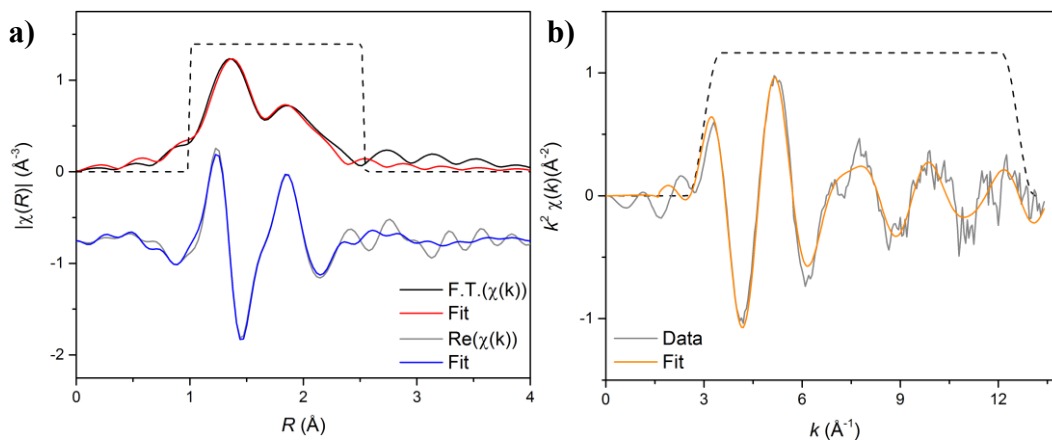
Figure S14 a) Fourier transform of the U L$_{III}$-edge EXAFS spectrum of n = 10 in *R*-space and fit (red trace). The real component and fit (blue trace) are presented beneath. b) EXAFS spectrum and fit (black trace) of n = 10 in *k*-space with accompanying fit. For both figures, the black dashed line denotes the fit window.
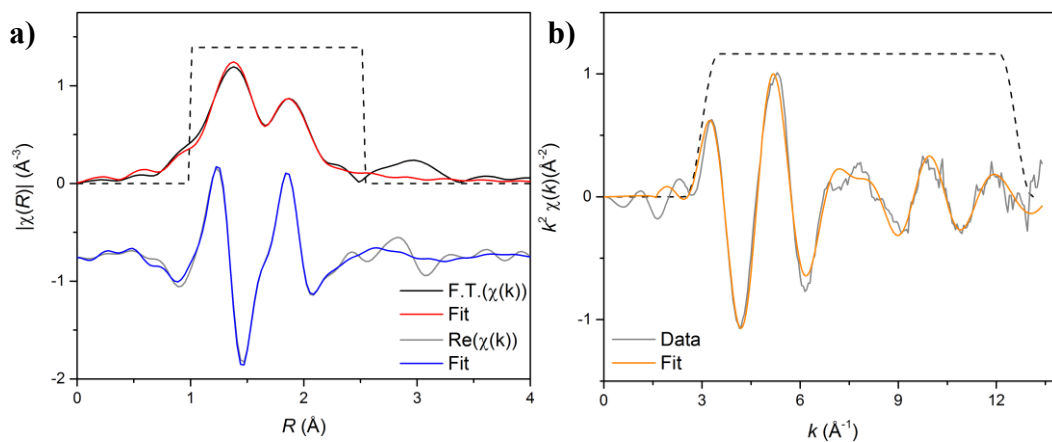
Figure S15 a) Fourier transform of the U L$_{III}$-edge EXAFS spectrum of n = 30 in *R*-space and fit (red trace). The real component and fit (blue trace) are presented beneath. b) EXAFS spectrum and fit (black trace) of n = 30 in *k*-space with accompanying fit. For both figures, the black dashed line denotes the fit window.
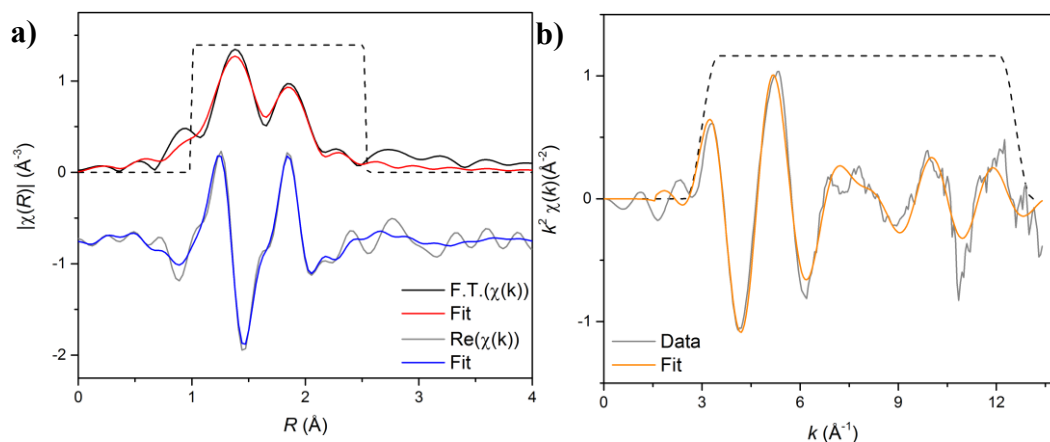
Figure S16 a) Fourier transform of the U L$_{III}$-edge EXAFS spectrum of for n = 125 in *R*-space and fit (red trace). The real component and fit (blue trace) are presented beneath. b) EXAFS spectrum and fit (black trace) of n = 125 in *k*-space with accompanying fit. For both figures, the black dashed line denotes the fit window.

Small Angle Neutron Scattering (SANS)

SANS data were collected on Beamline-6, EQ-SANS, at the Spallation Neutron Source of Oak Ridge National Laboratory.[9] Samples were prepared at a concentration of 10 mg mL^{-1} polymer in 15 mM $UO_2(NO_3)_2 \cdot 6\ H_2O$ in DMSO-d$_6$, and were transferred to quartz Helma cells possessing path lengths of 1 mm, then sealed with Teflon caps fastened with Parafilm. Data were collected at room temperature, with detectors located at 8 m, 4 m, and 1.3 m from the sample, corresponding to low, medium, and high q-range. The instrument was used in 60 Hz mode with minimum wavelengths of 10, 6, 1.5 Å, for 8m, 4m, and 1.3m detector locations respectively, to provide an effective *q*-range of ~ 0.003 Å^{-1} to 1.5 Å^{-1} Data were reduced and processed using MantidPlot using standard procedures to correct for detector sensitivity, instrument dark current, sample transmission and empty cell background.[10] Data fitting was performed using SasView 3.1.2 software (http://www.sasview.org).

Measured scattering intensities from all samples suggest very large structures whose length scale is beyond the instrument can reach. The lack of Guinier region of any of the measured scattering intensities prevents quantitative determination of the aggregate size from data fitting. For example,

scatterings from the shorted polymer chain and the longest polymer chain, which are representing the range of size changes in current experiment, can be speculated with a spherical aggregates model with polydispersity as shown in Figure S17. The calculation shows that measured data, regardless of polymer length, can be reasonably fitted with a spherical form factor model with any radius greater than 65 nm. Therefore, SANS data can be used to confirm existence of large aggregates and structural changes upon addition of metal ions but cannot be used to determine the size of the aggregates.
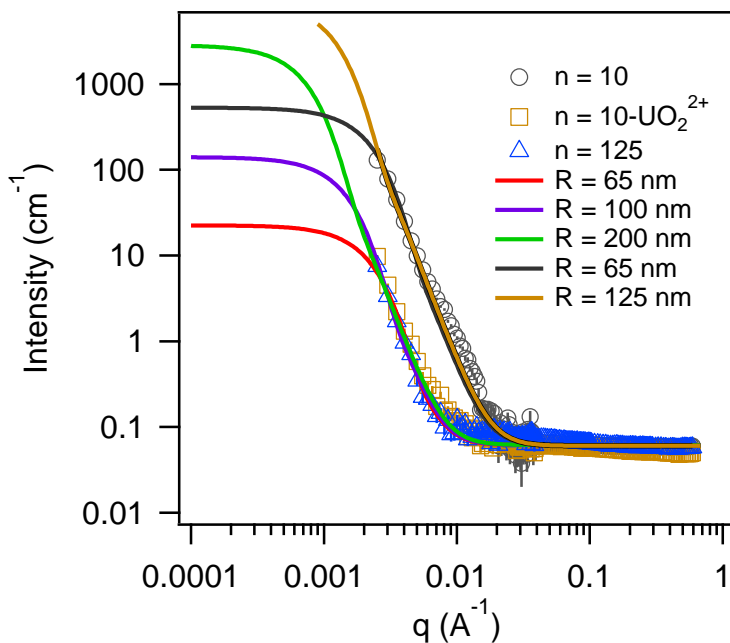
Figure S17. Model scattering curves for spheres with various radius with polydispersity (σ=0.3)

Dynamic Light Scattering:

Dynamic light scattering experiments were conducted at 25 ºC using an ALV compact goniometer system with 7002 Multiple Tau Digital Correlator. The wavelength of the incident light from the Helium-Neon laser was 632.8 nm. Disposable borosilicate glass culture tubes were used as sample cells and were cleaned prior to use within a reflux apparatus to remove dust. Samples were prepared at a concentration of 3 mg mL^{-1} polymer in 4.5 mM UO$_2$(NO$_3$)$_2$ · 6 H$_2$O in DMSO and filtered through a 0.45 μm PTFE filter.

The measured intensity autocorrelation functions were analyzed using the regularized inverse Laplace transform method with the ALV correlator software to obtain decay time distributions.

The hydrodynamic radius (R_h) of the polymers is obtained from the Stokes-Einstein relation and measured time decay from dynamic light scattering:

$$R_h = \frac{k_B T q^2 \tau}{6\pi\eta_s} = \frac{8\pi k_B T \, sin^2(\frac{\theta}{2}) n_0^2 \tau}{3\eta_s \lambda^2}$$

Where k_B is the Boltzmann constant, T is the absolute temperature, θ is the scattering angle, n_0 is the refractive index of the solvent, τ is the decay time obtained from the regularized inverse Laplace transform, η_s is solvent viscosity, and λ is the wavelength of incident light.

REFERENCES

1.   Oyola, Y.; Vukovic, S.; Dai, S., Elution by Le Chatelier's Principle for Maximum Recyclability of Adsorbents: Applied to Polyacrylamidoxime Adsorbents for Extraction of Uranium from Seawater. *Dalton T* **2016**, *45*, 8532-8540.

2.   Tang, C. B.; Kowalewski, T.; Matyjaszewski, K., Raft Polymerization of Acrylonitrile and Preparation of Block Copolymers Using 2-Cyanoethyl Dithiobenzoate as the Transfer Agent. *Macromolecules* **2003**, *36*, 8587-8589.

3.   Kopec, M.; Krys, P.; Yuan, R.; Matyjaszewski, K., Aqueous Raft Polymerization of Acrylonitrile. *Macromolecules* **2016**, *49*, 5877-5883.

4.   Webb, S. M., Sixpack: A Graphical User Interface for Xas Analysis Using Ifeffit. *Phys Scripta* **2005**, *T115*, 1011-1014.

5.   Ravel, B.; Newville, M., Athena, Artemis, Hephaestus: Data Analysis for X-Ray Absorption Spectroscopy Using Ifeffit. *J Synchrotron Radiat* **2005**, *12*, 537-541.

6.   Rehr, J. J.; Albers, R. C., Theoretical Approaches to X-Ray Absorption Fine Structure. *Rev. Mod. Phys.* **2000**, *72*, 621-654.

7.   Kelly, S. D.; Kemner, K. M.; Fein, J. B.; Fowle, D. A.; Boyanov, M. I.; Bunker, B. A.; Yee, N., X-Ray Absorption Fine Structure Determination of Ph-Dependent U-Bacterial Cell Wall Interactions. *Geochim. Cosmochim. Acta* **2002**, *66*, 3855-3871.

8.   Calvin, S., *Xafs for Everyone*; CRC Press: Boca Raton, FL, 2013.

9.   Zhao, J. K.; Gao, C. Y.; Liu, D., The Extended Q-Range Small-Angle Neutron Scattering Diffractometer at the Sns. *J. Appl. Crystallogr.* **2010**, *43*, 1068-1077.

10.   Arnold, O., et al., Mantid—Data Analysis and Visualization Package for Neutron Scattering and Sr Experiments. *Nucl. Instrum. Methods Phys. Res., Sect. A* **2014**, *764*, 156-166.